Nuclear Instruments and Methods in Physics Research A 1057 (2023) 168758

Contents lists available at ScienceDirect

Nuclear Inst. and Methods in Physics Research, A

journal homepage: www.elsevier.com/locate/nima

The large-area hybrid-optics CLAS12 RICH: First years of data-taking

M. Contalbrigo [a,*], L. Barion [a], M. Battisti [b], F. Benmokhtar [e], A. Boyer [e], C. Cuevas [c], P. Degtiarenko [c], C. Dickover [c], A. Kim [d], V. Kubarovsky [c], M. Mirazita [b], R. Malaguti [a], Z. Nickischer [e], D. Orecchini [b], C. Pecar [f], B. Raydo [c], P. Rossi [c,b], O. Soto [b], S. Tomassini [b], S. Vallarino [a]

[a] INFN Sezione di Ferrara and University of Ferrara, Italy
[b] INFN Laboratori Nazionali di Frascati, Italy
[c] Thomas Jefferson National Accelerator Facility, VA, USA
[d] University of Connecticut, CT, USA
[e] Duquesne University, PA, USA
[f] Duke University, NC, USA

ARTICLE INFO

Keywords:
Single-photon detection
Ring-imaging Cherenkov detectors
Front-end electronics
Multi-anode PMT
Digital readout

ABSTRACT

The CLAS12 deep-inelastic scattering experiment at the upgraded 12 GeV continuous electron beam accelerator facility of Jefferson Lab conjugates luminosity and wide acceptance to study the 3D nucleon structure in the yet poorly explored valence region, and to perform precision measurements in hadron spectroscopy. A large area ring-imaging Cherenkov detector has been designed to achieve the required hadron identification in the momentum range from 3 GeV/c to 8 GeV/c, with the kaon rate about one order of magnitude lower than the rate of pions and protons. The adopted solution comprises aerogel radiator and composite mirrors in a novel hybrid optics design, where either direct or reflected light could be imaged in a high-packed and high-segmented photon detector. The first RICH module was assembled during the second half of 2017 and installed at the beginning of January 2018, in time for the start of the experiment. The second RICH module, planned with the goal to be ready for the beginning of the operation with polarized targets, has been timely built despite the complications caused by the pandemic crisis and successfully installed in June 2022. The detector performance is here discussed with emphasis on the operation and stability during the data-taking, calibration and alignment procedures, reconstruction and pattern recognition algorithms, and particle identification.

1. The CLAS12 ring-imaging Cherenkov detector

The CLAS12 deep-inelastic scattering experiment [1] at Jefferson Lab (JLab) investigates the elementary building blocks of matter with a broad physics program, exploiting the scattering of a high-intensity polarized electron beam over (polarized) nuclear targets. To reach flavor sensitivity hadron identification in the final state is required [2]. A large-area ring-imaging Cherenkov (RICH) detector has been designed to achieve a pion rejection factor of the order of 1:500 in the momentum range from 3 GeV/c to 8 GeV/c at a luminosity as high as 10^{35} $cm^{-2}s^{-1}$. The adopted solution foresees a novel hybrid-optics design based on aerogel radiator, composite mirrors and a high-packed and high-segmented photon detector [3]. At CLAS12, two (out of six) radial sectors of the precedent gas Cherenkov detector are replaced with a RICH detector creating a symmetric setup useful to control the systematics in polarized reactions, see Fig. 1. Each RICH sector has a projective geometry, a gap depth of 1.2 m and about 5 m^2 entrance window area. A focusing mirror system has been designed to collect the light of large-angle particles and reduce the detection area instrumented by photon detectors to about 1 m^2 per sector, minimizing costs and influence on the detectors (time-of-flight TOF and Calorimeters) downstream of RICH, see Fig. 2.

As the inner volume is surrounded by mirrors, the Cherenkov light produced by a passing particle through the aerogel layer is imaged directly, or after one or multiple reflections. In particular, at large angles the light is focalized backward by the 3.5 m^2 spherical mirror, and reaches the detector plane after a second reflection by the front mirror supporting the aerogel, with a consequent second passage through the radiator, a distinctive feature of the CLAS12 RICH device.

* Corresponding author.
E-mail address: contalbrigo@fe.infn.it (M. Contalbrigo).

https://doi.org/10.1016/j.nima.2023.168758
Received 15 January 2023; Received in revised form 25 September 2023; Accepted 3 October 2023
Available online 6 October 2023

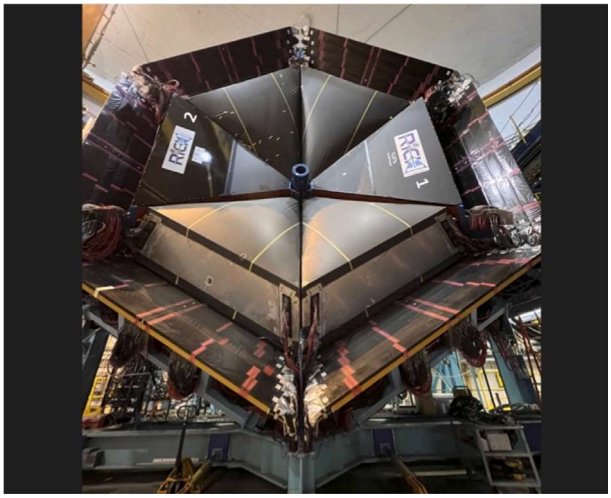

Fig. 1. The two CLAS12 RICH modules in a symmetric configuration.

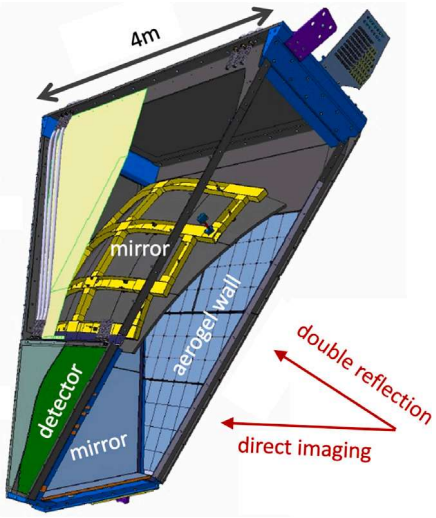

Fig. 2. 3D model of the RICH module.

The first RICH module (RICH1) was installed in January 2018 in time for the start of the CLAS12 data-taking. The second module (RICH2) was successfully completed in June 2022 despite the COVID restrictions, and as planned installed in time for the experiments with polarized targets.

2. RICH components

According to the symmetry concept, despite being built a few years apart, the two RICHes follow the same design and mount the same components. The aerogel layer is composed of 102 tiles produced by the Budker and Boreskov Institutes at Novosibirsk, and represent the world record so far achieved at n = 1.05 refractive index, both in volume, with a basic dimension of $20 \times 20 \times 3$ cm^3, and transparency, with a typical 50 mm scattering length at 400 nm [4]. The spherical mirrors are made from composite fiber reinforced polymers to ensure the wanted shape accuracy within a tolerance of 0.3 mrad, while limiting the material budget to less than 5 kg per squared meter. The planar mirrors exploit the cost-effective glass-skin technology derived from the terrestrial telescopes, with a sandwich of two thin glass layers and an Al honeycomb core, for the first time employed in a nuclear physics experiment. The glass thickness is reduced down to the exceptionally low value of 0.7 mm for the front mirrors inside the acceptance, and supporting the aerogel, in order to ensure a material budget corresponding to only about 1% of radiation length.

To reach the wanted spatial resolution of less than 1 cm, the flat panel Hamamatsu H8500 [5] multi-anode photo-multiplier (MAPMT) was selected thanks to the favorable geometry of 64 active pixels in a 5×5 cm^2 area with an effective 89% packing factor, in conjunction with the spectral response matching the aerogel useful wavelength range. At the beginning of the photosensor production the novel H12700 [5] MAPMT, with dynode structure optimized for single photon detection, became available and was adopted after thoughtful validation. With respect to the H8500, the H12700 MAPMT typically features a lower cross-talk and a 10% higher photon-detection efficiency despite the relative lower gain [6]. The CLAS12 RICH is the first large-area detector to employ this type of multi-anode photo-multiplier. A total of 391 MAPMTs, corresponding to about 25,000 pixels, are needed to cover the $\approx$ 1 m^2 trapezoidal active area in each RICH module. The typical gain is few 10^6, which corresponds to about 400 fC generated charge for a single photon-electron (SPE).

The front-end electronics is organized in compact units (tiles) mechanically designed to fit the MAPMT dimensions, each serving two or three MAPMTs for the best shaping of the tessellated surface and minimization of the dead space and services. A feed-through *adapter board* provides the bias (−1000 V) and the electrical connectivity of the sensors with the external readout system while preserving the adequate light and gas tightness of the detector. The *signal processing board* is based on the MAROC3 chip [7], whose 64 digital channels comprises a low impedance adjustable gain preamplifier followed by a fast shaper and an adjustable threshold discriminator to produce the start and stop logic pulse of each input signal. These are stored in a 8 μs deep circular memory awaiting the CLAS12 readout trigger and allowing a parallel, almost dead-time free, readout. The fast shaper works in an almost saturated regime to maximize the discrimination efficiency. A *FPGA board* provides the optical connection to the data acquisition system based on the customized Sub-System Processor (SSP) VME module designed at JLab. The current firmware version includes a 1 ns precision timestamping of the logic pulse, ensuring the sub-ns time resolution required to distinguish direct from reflected photon hits.

3. RICH readout

A constant-threshold binary readout requires an excellent stability of the baseline (pedestal) and working point (gain and threshold). Their programmed levels are here expressed as Digital-to-Analog Converter (DAC) units.

The time-over-threshold (ToT), derived from the recorded start and stop signal times, provides a non-linear estimate of the charge collected at the MAPMT anode. It could be used as a monitor of the stability over time of the MAPMT and readout chain performance (gain). No appreciable variations have been observed in the first years of operations. The ToT can be used to correct for the time-walk effect, a typical feature of the constant threshold readout. In order to have an easier handling of the time-walk and ToT behavior over the $\approx$ 50k channels of the RICH detector, an equalization of the SPE shaped pulses is desirable, in particular because the MAROC programmable threshold is common to all its 64 readout channels. The RICH channel-by-channel SPE signal equalization was performed using real data and allowed to compensate for the 1:4 typical variation of the MAPMT single pixel gain, see Fig. 3. After equalization, the ToT distribution of saturated SPE signals becomes narrower and better separated from the low-amplitude cross-talk signals. In Fig. 4, the typical measured dark rate of the H12700 pixel is plotted as a function of the discriminating threshold. The plot shows a large region of uniform response above a very narrow pedestal. The plateau is a consequence of the saturated mode employed in the MAROC binary readout and improves with gain

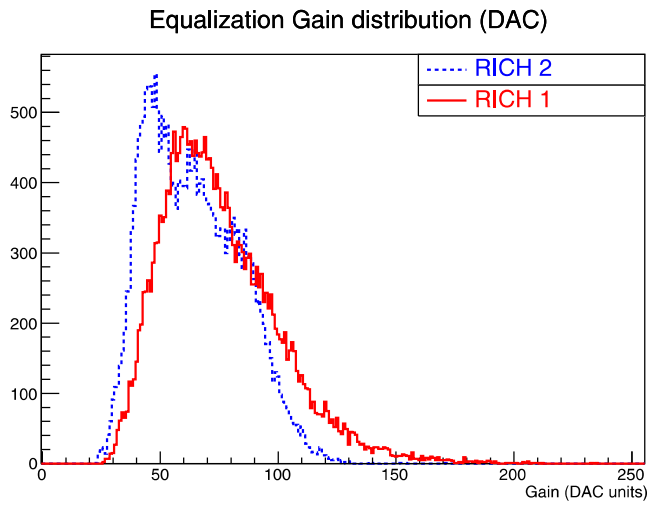

Fig. 3. Equalization gain distribution of the RICH readout channels. The gain is in DAC units, with 64 DAC meaning 1 (no gain change).

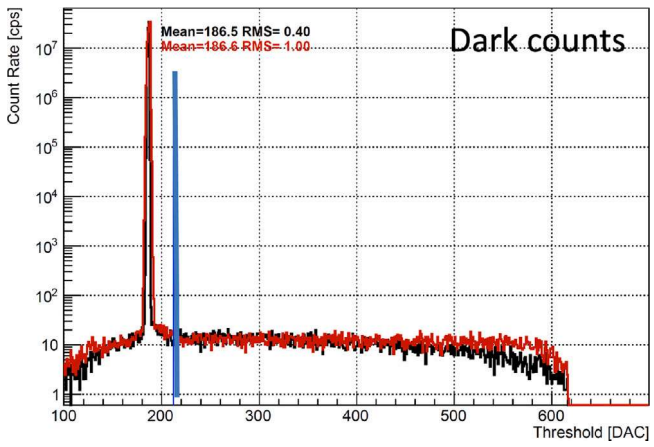

Fig. 4. Examples of dark counts as a function of the applied threshold before (black) and after (red) the gain equalization. Visible are the narrow pedestal and the wide plateau of almost constant efficiency for saturated signals, that support low threshold (with the reference value shown by the blue line) operation.

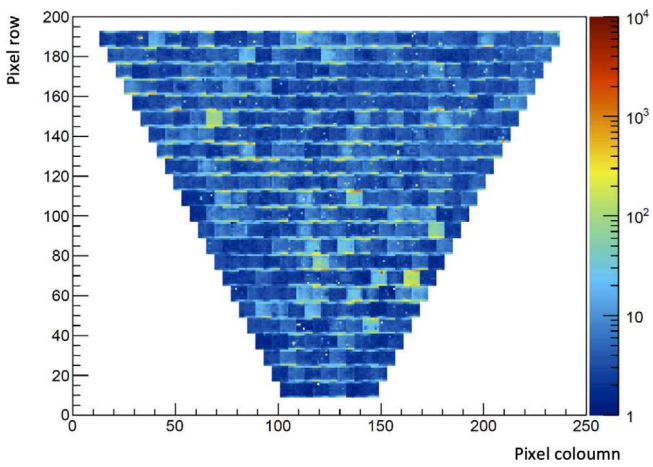

Fig. 5. Dark count map of the photo sensors of the second RICH module.

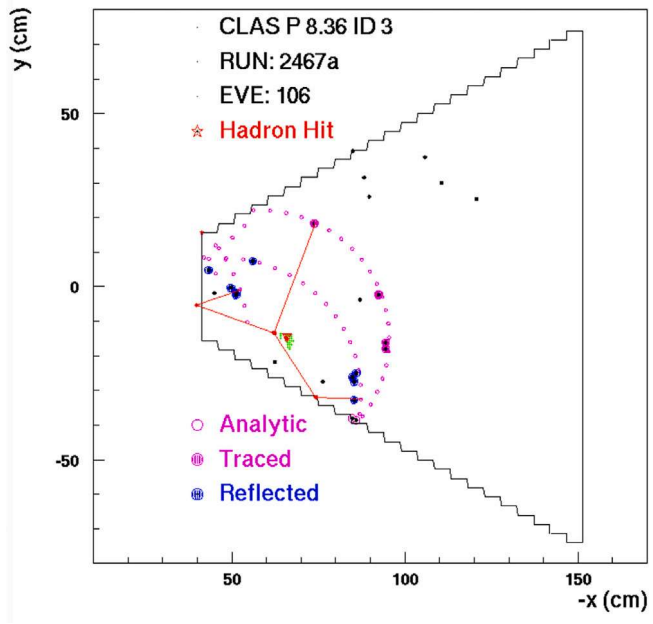

Fig. 6. Example of RICH reconstruction, see text. Visible are measured hits (small points), trials (open circles), reconstructed photons (full circles) and some ray-traced path (polylines).

equalization. It allows a flexible definition of the working point, a crucial feature when dealing with a large number of channels in the challenging single-photon regime.

The pedestal level is different for each MAROC, but is relatively uniform within one chip, a feature conforming to the common discrimination threshold. With HV ON, the typical measured dark count rate is below 100 Hz/pixel, in agreement with the Hamamatsu data-sheets, see Fig. 5. Only few (i.e. 10) channels show high dark rate (above 10 kHz) in RICH1 and none so far in RICH2. A consequence of the equalization and low dark count level is the capability to work at low threshold, corresponding to only $\approx 6\%$ of the single photon signal, ensuring high detection efficiency.

The time calibration is performed from real data, comparing the time measured at RICH with the flight time of the charged particle within CLAS12 (based on the high-precision TOF detector) and the flight time of the photons within the RICH (depending on the number of reflections and calculated by the RICH reconstruction procedure). After calibration, the typical single-photon time resolution is of the order of 0.6 ns.

4. Pattern recognition and particle identification

For each hit in the MAPMT plane, an estimate of the corresponding Cherenkov angle is derived by ray-tracing the photon path inside the RICH volume taking into account possible reflections [8]. The emission point is assumed to be the middle point of the hadron path inside the aerogel radiator. A limited number of photon (trials) are ray-traced for each particle hypothesis. For each measured hit, the closest trial is

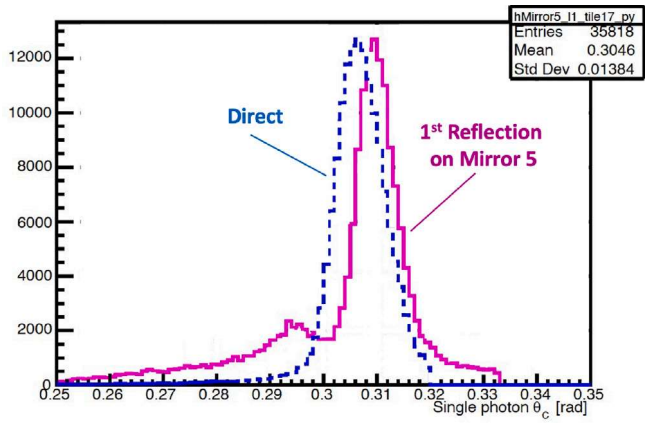

Fig. 7. Reconstructed angular distribution for direct and double reflected photons, the latter ones having the first-reflection on the central spherical mirror 5. The reflected photon distribution exhibits shifted populations due to different paths involving misaligned components, but similar width.

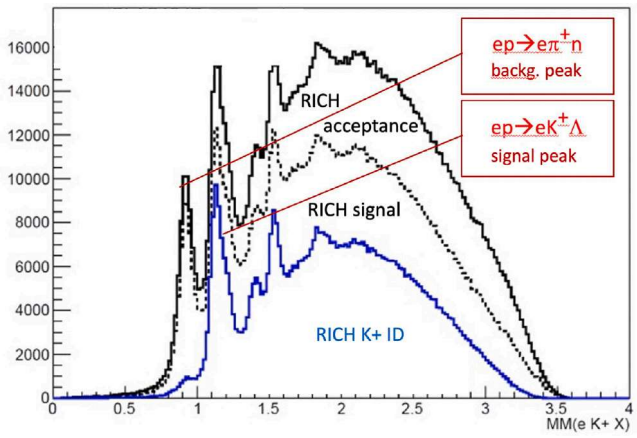

Fig. 8. Missing mass distribution for candidate events $ep \to e' K^+ X$ with the hadron in the RICH acceptance (black solid line), events with already available RICH information based on aligned components (black dashed line), and events with a confirmed kaon identification by RICH (blue line).

used to define the starting values of the hypothetical emission angles. Those are iteratively varied till the ray-traced hit and measured hit correspond, within a fraction of the expected angular resolution. The reconstructed path and angle are validated by a $\pm 3\sigma$ time coincidence between the RICH recorded time and the CLAS12 expected time. An example of a reconstructed RICH event is shown in Fig. 6. A distinct feature is the low level of spurious hits from accidentals, in-time background (i.e. Rayleigh scattering) and dark counts.

The Cherenkov analysis keeps the aerogel tiles as separated, as they have independent refractive index and geometry. The nominal aerogel parameters derived from laboratory characterization has to be cross-checked and validated with real data. A relevant example is the refractive index, that might vary with the environment (gas quality) and aerogel conditions. Electrons identified by other CLAS12 subsystems provide an excellent control sample for measuring the aerogel optical parameters, provided that the system is aligned. The alignment procedure is complicated due to the numerous involved components and various possible photon paths. After a backward reflection on the spherical mirror for example, there are several possible paths before the photons could be detected, depending on their emission angles and position. As a consequence, the alignment and subsequent refractive index calibration require a large statistical sample and the full classification of the various photon trajectories. This will become available with the upcoming CLAS12 data reprocessing now under preparation. The refractive index calibration should allow to get the same response (Cherenkov angle) irrespective of the particle charge or torus polarity.

The SPE Cherenkov angle resolution is of the order of 5 mrad in accordance with the expectations. This is true for the simple cases with none or just one reflection on the side mirrors, but also for the most complicated cases with multiple reflections (one of these on the spherical mirror), see Fig. 7. The RICH performance has been studied with the benchmark reaction $ep \to e' hX$. The missing mass distribution allows to identify specific reactions and therefore the produced hadron type. Of particular interest is the neutron peak corresponding to the charge exchange $ep \to e'\pi^+ n$, and the Lambda peak corresponding to the double-strange production $ep \to e' K^+ \Lambda$. Among the events with a candidate kaon in the CLAS12 RICH acceptance, reliable RICH information is available for the photon trajectories impinging on already aligned components. RICH data provide an effective identification, with a suppression of the fake charge-exchange peak and an improved signal over background ratio for the double-strange production, see Fig. 8.

5. Conclusions

The CLAS12 RICH has been completed with the installation of the second module in time for the experiments with polarized targets. The first module has been operated since 2018, showing an excellent stability over time. Calibration in time and refractive index allowed to approach the design resolution for both direct and reflected light topologies. With the upcoming CLAS12 data reprocessing, a complete alignment accounting for the most involved photon paths, and therefore the reach of the full particle identification capability, is expected.

Declaration of competing interest

The authors declare that they have no known competing financial interests or personal relationships that could have appeared to influence the work reported in this paper.

Acknowledgments

This material is based upon work supported by INFN, Italy, the European Union's Research and Innovation programs under Grant Agreement N.824093 (STRONG2020) and N.101003460 (PROBES), and by the U.S. Department of Energy, Office of Science, Office of Nuclear Physics under contract DE-AC05-06OR23177 and the National Science Foundation, United States, Award #2012413. We thank the JLab Detector Support Group and Fast Electronic Group, the Hall-B technical and management staff and the INFN technical and administrative service.

References

[1] V.D. Burkert, et al., Nucl. Instrum. Methods A 959 (2020) 163419.
[2] H. Avakian, et al., 2012. arXiv:1202.1910v2 [hep-ex].
[3] M. Contalbrigo, et al., Nucl. Instrum. Methods A 964 (2020) 163791.
[4] M. Contalbrigo, et al., Nucl. Instrum. Methods A 876 (2017) 168.
[5] https://www.hamamatsu.com.
[6] P. Degtiarenko, et al., Nucl. Instrum. Methods A 1044 (2022) 167446.
[7] S. Blin, et al., IEEE Nucl. Sci. Symp. Conf. Rec. 2010 (2010) 1690.
[8] V. Ziegler, et al., Nucl. Instrum. Methods A 959 (2020) 163472.